Published in final edited form as:
Nat Genet. 2013 August ; 45(8): 927–932. doi:10.1038/ng.2682.

Recurrent somatic alterations of *FGFR1* and *NTRK2* in pilocytic astrocytoma

A full list of authors and affiliations appears at the end of the article.

Abstract

Pilocytic astrocytoma, the most common childhood brain tumor[1], is typically associated with mitogen-activated protein kinase (MAPK) pathway alterations[2]. Surgically inaccessible midline tumors are therapeutically challenging, showing sustained tendency for progression[3] and often becoming a chronic disease with substantial morbidities[4].

Here we describe whole-genome sequencing of 96 pilocytic astrocytomas, with matched RNA sequencing (n=73), conducted by the International Cancer Genome Consortium (ICGC) PedBrain Tumor Project. We identified recurrent activating mutations in *FGFR1* and *PTPN11* and novel *NTRK2* fusion genes in non-cerebellar tumors. New *BRAF* activating changes were also observed. MAPK pathway alterations affected 100% of tumors analyzed, with no other significant mutations, indicating pilocytic astrocytoma as predominantly a single-pathway disease.

Notably, we identified the same *FGFR1* mutations in a subset of *H3F3A*-mutated pediatric glioblastoma with additional alterations in *NF1*[5]. Our findings thus identify new potential therapeutic targets in distinct subsets of pilocytic astrocytoma and childhood glioblastoma.

Pilocytic astrocytoma is the most common central nervous system (CNS) neoplasm in childhood, accounting for ~20% of all pediatric brain tumors. Tumor locations in our cohort reflect the fact that pilocytic astrocytomas occur throughout the CNS, with about half arising outside the cerebellum (Supplementary Figure 1). Extra-cerebellar tumors are often

Correspondence and requests for materials should be addressed to R.E. (r.eils@dkfz-heidelberg.de), P.L. (m.macleod@dkfz-heidelberg.de) or S.M.P (s.pfister@dkfz-heidelberg.de).
*These authors contributed equally
#These authors contributed equally
38http://www.pedbraintumor.org

URLs
1000 Genomes Project: http://www.1000genomes.org/
GenomeMuSiC: http://gmt.genome.wustl.edu/genome-music/0.2/index.html

Accession codes
Sequencing data have been deposited at the European Genome-phenome Archive, which is hosted by the European Bioinformatics Institute (EBI), under accession EGAS00001000381.

Supplementary Information is available in the online version of the paper.

Author Contributions
D.T.W.J., S.R.L., D.A.K.Q., A.M.F., H-J.W., A.M.S., S.H., M.Zu., J.G., S.Sch., H.Ş -C., H.W., S.B., E.P., S.St., B.R., D.F., C.C.B., C.v.K., P.v.S, R.Ve., M.Su., S.W., M.H., and J.F. performed and/or coordinated experimental work.
B.H., N. Jäger, D.T.W.J., M.Ko., H-J.W., T.Z., B.L., P.A.N., V.H., J.S., J.M., M.Za., M.Sch., C.L.W., C.D.V., S.R., C.L., P.v.S., J.K., R.Vo, and M.Ra. performed data analysis.
A.K., M.Ry., C.M., B.W., A.U., C.H-M., T.M., A.E.K., M.E., M.U.S., Y-J.C., S.L.P., A.v.D., O.W., M.H., M.A.K., C.G.E., W.S., K.L.L., M.W.K., V.P.C., and N.Jabado collected data and provided patient materials.
D.T.W.J., B.H., N. Jäger, D.S., N. Jabado, R.E., P.L. and S.M.P. prepared the initial manuscript and figures.
A.K., U.D.W., M.D.T., J.O.K., H.L., M-L.Y., B.B., G.R., V.P.C., N. Jabado, R.E., P.L. and S.M.P. provided project leadership.
All authors contributed to the final manuscript

The authors declare no competing financial interests.

surgically inaccessible, leading to a chronic disease with multiple recurrences, visual and neurological impairment, and/or side-effects of therapy[1,4]. Genetic alterations within the MAPK signaling pathway are a hallmark of this tumor, with *KIAA1549:BRAF* fusion being the most frequent event[6–8]. A smaller number harbor *BRAF* or *KRAS* point mutations, alternative *BRAF*/*RAF1* fusions, or germline *NF1* mutations[2]. Pilocytic astrocytoma has therefore been hypothesized to represent a single-pathway disease[2]. Previously, however, no MAPK pathway changes were identifiable in 15–20% of tumors (mostly non-cerebellar).

To investigate the full range of genetic alterations in pilocytic astrocytoma, we performed whole-genome sequencing of tumor and blood DNA from 96 patients (Supplementary Table 1). Corresponding RNA sequencing data and larger insert mate-pair sequencing (for enhanced structural rearrangement detection) were generated for 73 and 68 samples, respectively. The average somatic mutation rate was extremely low (<0.1/Mb), with a mean of 1.6 non-synonymous single nucleotide variants (SNVs) per tumor (range 0–9; Supplementary Table 1) – similar to the rate described in NF1-associated pilocytic astrocytomas[9]. This is markedly lower than recently reported for the malignant pediatric brain tumor medulloblastoma[10–12], and several other pediatric solid tumors[13]. The average number of small insertions/deletions (InDels) affecting coding sequences was <1 per case. All coding somatic SNVs/InDels are listed in Supplementary Table 2.

In line with other tumor types[10,14,15], genome-wide mutation rates positively correlated with patient age ($r = 0.42$, $P = 2.3 \times 10^{-5}$, Pearson's product-moment correlation; Supplementary Figure 2a). The observed mutations were predominantly C-to-T transitions at CpG sites (likely deamination of methylated cytosines), suggesting that the age-dependent increase may largely be due to background processes occurring in progenitor cells prior to tumorigenesis, as recently reported in leukemia[15] (Supplementary Figure 2b).

Most of the known MAPK pathway activating events were also found in this series, including *KIAA1549:BRAF* fusion variants (70 cases), a *FAM131B:BRAF* fusion[16], four $BRAF^{V600E}$ mutations and one $BRAF^{ins599T}$ (Supplementary Table 1). Three tumors were associated with Neurofibromatosis Type 1. This is fewer than would be expected for prospective cohorts (5–10%), since material for biological studies from these typically optic pathway-associated tumors is limited. *NF1* has been reported to follow a classical tumor suppressor model in pilocytic astrocytoma, with a somatic second hit in addition to the germline alteration[9]. This also held true in our series (Supplementary Table 1).

Analysis of copy number and structural alterations using DNA and RNA sequencing revealed four novel *BRAF* fusions (Figure 1, Supplementary Figure 3). As expected, all variants resulted in loss of the amino-terminal regulatory region of BRAF. An *RNF130:BRAF* fusion derived from a reciprocal t(5;7)(q35;q34) translocation was seen in two cases (Figure 1a), with single examples of *CLCN6:BRAF*, *MKRN1:BRAF* and *GNAI1:BRAF* fusions (Supplementary Figure 3a–c). Thus, non-*KIAA1549:BRAF* fusions comprise a significant minority of activating events, with BRAF apparently being a promiscuous fusion partner.

Another new *BRAF* alteration was identified in ICGC_PA65, resulting in a three amino acid insertion (p.R506_insVLR) in the interdomain cleft of BRAF - a structural region linked to its activity[17] and homodimerization[18]. Protein modeling predicted that these residues stabilize a dimeric form of BRAF (known to be active independent of RAS stimulation[19]) (Figure 1b). Homodimerization was confirmed by immunoprecipitation, and the $BRAF^{insVLR}$ mutant increased ERK phosphorylation as effectively as $BRAF^{V600E}$ (Figure 1c,d).

Novel alterations in *KRAS* were also observed. ICGC_PA117 and ICGC_PA142 both showed two distinct mutations (E63K/R73M and L19F/Q22K, respectively). DNA and RNA-seq data confirmed that both alterations affected the same allele (Supplementary Figure 4). Whilst there are reports of double *KRAS* mutations in entities such as colon cancer[20], these typically involve at least one hotspot residue (codons 12, 13 or 61), and often represent heterogeneous tumor subclones rather than two hits in one allele (although this has also been described, e.g. [21]). The alterations seen in our tumors do not encompass classical hotspots, suggesting that further characterization of downstream effects is warranted.

All but one of the cerebellar tumors in our series harbored a *BRAF* fusion, with the other displaying a *KRAS* alteration. 9/48 (19%) of the non-cerebellar tumors, however, lacked any of the above alterations. Further assessment of structural rearrangements revealed two novel gene fusions in a total of 3 samples, involving the kinase domain of *NTRK2* (also known as *TrkB*) - an oncogene implicated in the tumorigenesis of neuroblastoma, amongst others[22,23]. The related *NTRK1* and *NTRK3* genes have previously been shown to be activated by fusion events (e.g. *TPM3:NTRK1* in papillary thyroid cancer[24] and *ETV6:NTRK3* in multiple tumors[25]). The *QKI:NTRK2* and *NACC2:NTRK2* fusions identified here were verified by PCR (Figure 2, Supplementary Figure 3d). Both 5′ partners contain dimerization domains, and are therefore predicted to induce ligand-independent dimerization. Interestingly, N-terminal TrkB truncation has recently been shown to induce transformation of neural crest cells[26]. The downstream effects of TrkB activation are mediated at least in part via MAPK pathway activation[27].

A second new recurrent alteration, namely mutation of two hotspot residues (N546 & K656) in the kinase domain of FGFR1, was seen in five tumors (Supplementary Table 3 and Figure 3a). *FGFR1* is more commonly activated through amplification, in tumors such as breast[28] and lung[29,30] cancer. Occasional *FGFR1* mutations have been observed in adult glioblastoma (GBM)[31,32], a highly malignant astrocytoma, as have *FGFR1:TACC1* or *FGFR3:TACC3* fusion genes[33]. Mutations in homologous codons in *FGFR2* and *FGFR3* are commonly found in other tumor types, particularly bladder, skin and endometrial cancers (see the COSMIC database[34]). Both mutations result in midbrain hyperproliferation in developing chick embryos[35]. The N546K mutation alters FGFR1 auto-phosphorylation, resulting in increased kinase activity and transforming potential[36], while the K656E variant is also transforming *in vitro*[37]. Interestingly, the latter study suggested that FGF2 (bFGF) ligand was necessary in addition to *FGFR1* mutation to maintain neurosphere formation *in vitro*. Gene expression array data of 118 pilocytic astrocytomas, including 66 from the present series, revealed significantly increased *FGF2* expression in pilocytic astrocytoma compared with 158 other astrocytic tumors[38,39], or normal tissues[40]. This increase was not restricted to only *FGFR1*-mutant or wild-type tumors, suggesting that ligand-mediated pathway activation may play a general role in tumorigenesis (Figure 3b). Immunohistochemical detection of phospho-FGFR1 revealed strong, diffuse positivity in all seven pilocytic astrocytomas harboring an *FGFR1* mutation for which material was available. No positivity was observed in eleven *FGFR1*^{WT} tumors. All samples displayed strong phospho-ERK staining (Supplementary Figure 5). Interestingly, ICGC_PA89 harbored an alternative alteration in *FGFR1*, consisting of a ~4.5kb internal tandem duplication (ITD) of the portion of the gene encoding the kinase domain, reminiscent of the activating internal tandem duplications of the *FLT3* kinase observed in acute myeloid leukemia[41] (Figure 3c).

Further recurrent alterations were found in a RAS/MAPK-related adaptor protein, the phosphatase PTPN11 (also called SHP-2, Figure 3c). Both alterations (E69K and E76A) were previously reported in juvenile monomyelocytic leukemia, which is frequently associated with SHP-2 activation[42,43]. Interestingly, both were found in *FGFR1*-mutant

tumors (ICGC_PA84 & ICGC_PA166), suggesting a cooperative role in tumorigenesis (Supplementary Table 3). Overexpression of mutant SHP-2 alone did not elevate pERK levels *in vitro*, while the two FGFR1 mutants, either alone or in combination with mutant SHP-2, upregulated pERK (Supplementary Figure 6). This would support the hypothesis that *PTPN11* mutation alone is insufficient for pilocytic astrocytoma development, but that it may play a modifying role in *FGFR1*-mutant tumors. Of note, *PTPN11/SHP-2* expression was increased in pilocytic astrocytomas when compared with other astrocytomas or normal tissues (Figure 3d), suggesting a broader role in the biology of this entity. An additional cohort of 45 non-cerebellar pilocytic astrocytomas, negative for *KIAA1549:BRAF*, was screened for *FGFR1* (exons 12 & 14) and *PTPN11* (exon 3) mutations. Nine cases harbored FGFR1 mutations at N546 or K656, and one additionally carried a PTPN11/SHP-2 E69K change (Supplementary Table 3), confirming our whole-genome sequencing findings. Germline *PTPN11* mutations are one of the causes of the hereditary developmental disorders Noonan syndrome (NS)[44] and LEOPARD syndrome (LS)[45]. A few case reports have described pilocytic astrocytomas occurring in NS and LS patients[46–49]. Together with NF1, this makes three known 'RASopathies', characterized by germline MAPK pathway mutations[50], linked with pilocytic astrocytoma tumorigenesis. In our germline sequencing data, however, *NF1* was the only RASopathy gene disrupted at a higher frequency than in the 1000 Genomes Project (URL below).

Strikingly, all of the pilocytic astrocytomas in our cohort harbored a MAPK pathway alteration. *BRAF*, *FGFR1*, *KRAS* and *NF1* were the only genes found to be significantly mutated using the Genome MuSiC algorithm (URL below, Supplementary Table 4). With the exception of *FGFR1* and *PTPN11*, each case typically harbored only one pathway alteration ($P < 0.0001$, permutation test, Figure 4). Together with the finding that BRAF kinase activation alone is sufficient to induce pilocytic astrocytomas in mice[51,52], these data strongly support the concept of pilocytic astrocytoma as a prototypic single-pathway disease driven by a limited number of oncogenic hits (possibly only one in some cases; Supplementary Figure 7).

Interestingly, one of the *FGFR1*-mutant tumors (ICGC_PA69) also displayed an H3F3A K27M mutation and somatic alterations of *NF1* – both of which are more commonly encountered in pediatric glioblastoma (GBM)[5]. Three experienced neuropathologists (AK, GR and JF) reported pilocytic astrocytoma histology for this case, although a diagnosis of GBM cannot be conclusively excluded due to limited material. By examining previous exome sequencing data for pediatric GBM[5], we identified 3/48 samples (6%) with an *FGFR1* mutation. Strikingly, all three harbored the same constellation of H3F3A K27M, somatic *NF1* alteration, and *FGFR1* activation (Supplementary Table 3). They were also wild-type for *TP53*, which is mutated in most K27M-mutant GBM or diffuse intrinsic pontine gliomas[5,53]. One tumor reported in a targeted sequencing cohort of medulloblastoma[10] had a similar triplet, with H3F3A K27M, *NF1* mutation and an FGFR2 K659E mutation (homologous to FGFR1 K656E), making a total of 5 cases with this triple-mutation combination. Gene expression analysis indicated that this is likely a GBM previously mis-classified as medulloblastoma. It is not currently clear why these mutations occur in concert, and additional work will be required to assess their roles. One possibility is that *NF1* mutation may mimic elevated *PTPN11* expression, since activation of PTPN11/SHP-2 inhibits the recruitment of Ras GTPase-activating proteins (RasGAPs, including NF1) to the plasma membrane[54].

All *FGFR1*-mutant tumors were extra-cerebellar, mostly in midline locations (Supplementary Table 3), suggesting a link between cell of origin and/or microenvironment with *FGFR1*-driven tumorigenesis. The H3F3A K27M mutation is also associated with midline GBM[39]. Notably, *FGFR1* plays a role in neural stem cell self-renewal[55], and is

essential for midline glial cell development[56]. This spatial clustering may also reflect differential sensitivity of distinct neural precursors to activating stimuli, particularly *NF1* loss[57,58]. The type and timing of second hits (*H3F3A*/*NF1* mutation) and/or the differentiation stage of the cell of origin may contribute to determining a fate of oncogene-induced senescence and slow growth (pilocytic astrocytoma)[59,60] versus aggressive malignancy with poor outcome (GBM).

In summary, this study has identified new insights into the tumorigenesis of pilocytic astrocytoma. Each tumor harbored very few mutations, in keeping with a generally benign behavior. Importantly, our findings confirm the concept that pilocytic astrocytomas are predominantly driven by aberrant activation of the MAPK pathway. Most strikingly, however, we report novel recurrent alterations in *NTRK2*, *FGFR1* and *PTPN11*, which were mutually exclusive with other *RAF/RAS* alterations. Combined with the observation of *FGF2* and *PTPN11* overexpression, these results indicate upstream contributors to MAPK pathway activation in this entity. Emerging preclinical data suggest that BRAF inhibitors may trigger paradoxical activation in tumors harboring *KIAA1549:BRAF*, i.e. the majority of pilocytic astrocytomas[61]. Single-drug or combination therapy with FGFR, NTRK2 and/or MEK inhibitors, several of which are currently in preclinical and clinical trials[62–64], may therefore represent rational treatment options. $BRAF^{V600E}$-specific agents may also be a logical choice for ~5% of patients. Finally, the identification of recurrent *FGFR1* mutations in a subset of pediatric GBM provide an opportunity for therapeutic targeting of FGFR signaling in these clinically challenging brain tumors.

Methods

Sample collection

Informed consent and an ethical vote (Ethics Committee of the Medical Faculty of Heidelberg) were obtained according to ICGC guidelines (http://www.icgc.org). Tumor tissues were subjected to neuropathological review to confirm histology and tumor cell content.

DNA Sequencing

Paired-end library preparation was conducted using Illumina, Inc. v2 protocols. 1–5μg of genomic DNA were fragmented to ~300 bp insert-size with a Covaris device, followed by size selection through agarose gel excision. Mate-pair (long-range paired-end mapping) DNA library preparation was carried out using the v2 protocol from Illumina. 10ug of genomic DNA were fragmented to 4.5kb with a Hydroshear device, followed by size selection. Deep sequencing was carried out with Illumina HiSeq2000 instruments.

RNA Sequencing

Twenty-three RNAseq libraries were prepared with purified polyA+ RNA fractions using strand-specific methods, following dUTP-based protocols as described in[65], featuring cDNA fragmentation after mRNA priming with random hexamers (dN)6 and oligo(dT) primers. Six libraries were constructed with a modified protocol whereby the polyA+ fraction was fragmented using RNA fragmentation reagents (Ambion, Cat. #AM8740); first strand synthesis was then performed with random hexamers only (cDNA fragmentation was omitted). Fifty RNAseq libraries were prepared with a ribosomal RNA-depleted fraction. In brief, 0.2 μg of total RNA was prepared using the RiboZero™ Gold kit (Epicentre). The resulting RNA was further processed following the library preparation protocol described in [66], starting at the fragmentation step (2^{nd} step). Sequencing (2×51bp) was carried out on the HiSeq2000.

Mapping and analysis

Sequencing reads were mapped and aligned to the hg19 reference assembly as previously described[10], using BWA[67] (version 0.5), and processed with samtools[68] (version 0.1.17) and Picard tools (version 1.61).

An in-house analysis pipeline based on samtools mpileup and bcftools[68] was used to detect single nucleotide variants (SNV) and small insertions or deletions (InDels). In addition to previously described filters to remove artefacts[10], we excluded variants located in regions of low mappability or overlapping with the hiSeqDepthTop10Pct, Encode DAC Blacklisted Regions, or Duke Excluded Regions tracks from UCSC genome browser. High confidence somatic SNVs were not allowed to overlap with any two of the following features: tandem repeats, simple repeats, low complexity, satellite repeats, or segmental duplications. In addition, following heuristic criteria were applied: (1) at least 5 tumor reads at the position; (2) more than one variant read per strand, or at least 5 variant reads in total and variant allele fraction > 0.1; (3) at least 12 reads at the position in the matching control; (4) less than 1/30 of the control reads supporting the variant; (5) less than 300 reads at the corresponding position in the control; (6) no non-reference, non-variant bases at the corresponding position in the control.

InDels were called with samtools mpileup and bcftools on reads with mapping quality >20 and scored in a similar way as SNVs. Overlap with tandem or simple repeats, however, was not penalized, since these elements are prone to InDels due to polymerase slippage. Since InDel alignments in the matched control can be slightly shifted in comparison to the tumor, or mismatches preferred over gaps, germline events can be falsely called as somatic. We therefore required not more than one mismatch or InDel in the control within 20bp of the tumor InDel.

Tumor and matched control samples were also analyzed with Pindel (version 0.2.4h)[69]. Events in the tumor were only considered when supported by at least five reads and if the number of supporting reads divided by the maximum of the read depth at the left and right breakpoints was >0.05. The matched control sample was also analyzed by samtools mpileup at tumor InDel positions and 10bp up- and downstream. Variants were classified as somatic if both Pindel and samtools mpileup did not call a multibase variant in the control sample. Only additional InDels in “RASopathy” genes were reported from the Pindel analysis (due to a high false positive rate), all other InDels were called with samtools as described above.

SNVs and InDels were functionally annotated with RefSeq gene annotations using Annovar[70] and Oncotator (http://www.broadinstitute.org/oncotator/). For the identification of significantly mutated genes we used the high confidence somatic SNVs and InDels as input for Genome MuSiC[71] (version 0.3), setting max-fdr to 0.05 in the genome music smg module. Substitution patterns of SNVs were evaluated in a sequence context of all 96 possible trinucleotides to assess mutational signatures[72].

Integration of SNVs and InDels with RNAseq data

Gene expression levels were calculated per-exon according to reads per kilobase of exon model per million mapped reads (RPKM) using BedTools[73] and custom Perl scripts. Where available, candidate DNA variant positions were annotated with RNA information by generating a pileup of the DNA variant position in the RNA BAM file (Supplementary Table 2).

Structural rearrangement detection & verification

Rearrangements based on paired-end data were identified using read-depth analysis, CREST[74], DELLY[75], and manual inspection of sequencing reads. Rearrangements based on mate-pair data were identified using DELLY and manual inspection of sequencing reads, as previously described[10].

Structural variants were verified by PCR (conditions and primer sequences available upon request). PCR products were sent to GATC Biotech (Germany) for Sanger sequencing to confirm breakpoints.

Fusion transcript detection & verification

Fastq files from transcriptome sequencing were used for *de novo* annotation of fusion transcripts using the TopHat-Fusion[76] and deFuse[77] algorithms with standard parameters. Where neither algorithm detected fusions, but whole-genome sequencing supported a fusion, we extracted corresponding transcriptome reads matching the theoretical sequence surrounding the predicted fusion border and then counted as fusion reads those where the entire 51bp sequences were derived from the predicted fused exons.

Primers for amplification of neighboring exons in normal (unfused) transcripts were tested in RT-PCR using total RNA from normal cerebellum (BioChain, lot number B307003). Validated primers were used to amplify the normal transcripts (control) and fusion transcripts from tumor RNA using the SuperScript III One-Step RT-PCR System with Platinum *Taq* DNA Polymerase (Invitrogen). PCR conditions and primer sequences are available upon request.

Computational protein modeling

A dimeric model of mutant $BRAF^{insVLR}$ was produced with Modeller[78] using the PDB structure 4E26 as a template. Ten models were produced, with the one having the lowest DOPE score shown in main Figure 1b.

Expression Array Analysis

Affymetrix U133 Plus2.0 expression array data for genes of interest were extracted from publicly-available datasets via the R2 software tool (http://r2.amc.nl), and for additional cases on an early-access basis through collaboration with the Microarray Department of the University of Amsterdam, the Netherlands. The MAS5.0 algorithm of the GCOS program (Affymetrix Inc) was used for normalization and assignment of detection p-values. Array quality was ensured by inspection of beta-actin and GAPDH 5′-3′ ratios as well as the percentage of present calls.

Verification of SNVs/InDels

All SNVs/InDels in *FGFR1*, *PTPN11*, *BRAF*, *KRAS*, *NF1* and *H3F3A* were verified by PCR followed by capillary (Sanger) sequencing. Additional variants were also verified in this way, as listed in Supplementary Table 2. Verification rates for SNVs was >98%, and for InDels was >70%. Alterations determined to be false are not included in Supplementary Table 2.

In vitro and protein assays

Coding sequences of *BRAF*, *PTPN11* and *FGFR1* were cloned from normal brain cDNA (Stratagene) into a pcDNA3.1 vector with HA, FLAG or AU1 epitope tags. Site-directed mutagenesis (QuikChangeII XL, Agilent Technologies) was used to generate $BRAF^{V600E}$, $BRAF^{insVLR}$, $PTPN11^{E69K}$, $PTPN11^{E76A}$, $FGFR1^{N546K}$ and $FGFR1^{K656E}$.

NIH3T3 murine fibroblasts (Leibniz Institute DSMZ, Germany; mycoplasma tested) were cultured in DMEM (Life Technologies), 10% FBS (Life Technologies) and penicillin/streptomycin at 37°C in 5% CO_2. Cells were transfected using Lipofectamine® 2000 diluted in Opti-MEM® (Invitrogen), and switched to serum-free DMEM 24h after transfection. After a further 24h, cells were lysed in either RIPA buffer or RLT buffer (Qiagen). Protein electrophoresis was performed using 4–12% gradient NuPAGE Bis-Tris Precast Gels (Life Technologies) with transfer to a PVDF membrane. Antibodies for Western blotting, with detection using ECL (GE Healthcare Life Sciences), were as follows: anti-ERK1/2 (rabbit polyclonal, Cell Signaling Technology #9102), anti-phospho-ERK1/2 (rabbit monoclonal 20G11, Cell Signaling Technology #4376), anti-HA (rabbit monoclonal C29F4, Cell Signaling Technology #3724), anti-AU1 (rabbit polyclonal, Abcam ab3401), anti-DYKDDDDK (FLAG®) (rabbit polyclonal, Cell Signaling Technology #2368), HRP-conjugated goat anti-Rabbit IgG (Santa Cruz Biotechnology, sc-2004), HRP-conjugated goat anti-mouse Ig (Santa Cruz Biotechnology, sc-2005).

For co-immunoprecipitation (Co-IP) to assess BRAF dimerization, cells were washed twice in ice-cold PBS, scraped, pelleted, and then lysed on ice in 5 pellet-volumes of lysis buffer (50mM HEPES, pH7.5; 250mM NaCl; 1mM EDTA; 2,5 mM EGTA; 10% Glycerol; 0.1% Triton X-100; protease inhibitors) with regular vortexing. Lysates were run through a QiaShredder column (Qiagen), centrifuged, and transferred to a new tube. 8μl of anti-HA agarose slurry (Thermo Scientific) were washed 3 times then resuspended in 20μl lysis buffer. 50μg protein extract was added to the anti-HA slurry and rotated overnight at 4°C. Finally, beads were pelleted, washed seven times in lysis buffer, and resuspended in SDS sample buffer for Western blotting.

Immunohistochemistry (IHC)

IHC was performed with an automated stainer (Benchmark XT; Ventana). Phospho-FGFR (Y653/Y654) was assessed using antibody PA5-12594 (Thermo Scientific), diluted 1:50. Phospho-ERK1/2 (T202/Y204) was assessed using antibody #9101 (Cell Signaling Technology), diluted 1:100.

Supplementary Material

Refer to Web version on PubMed Central for supplementary material.

Authors

David T.W. Jones[1,*], Barbara Hutter[2,*], Natalie Jäger[2,*], Andrey Korshunov[3,4], Marcel Kool[1], Hans-Jörg Warnatz[5], Thomas Zichner[6], Sally R. Lambert[7], Marina Ryzhova[8], Dong Anh Khuong Quang[9], Adam M. Fontebasso[9], Adrian M. Stütz[6], Sonja Hutter[1], Marc Zuckermann[10], Dominik Sturm[1], Jan Gronych[10], Bärbel Lasitschka[11], Sabine Schmidt[11], Huriye Şeker-Cin[1], Hendrik Witt[1,12], Marc Sultan[5], Meryem Ralser[5], Paul A. Northcott[1], Volker Hovestadt[10], Sebastian Bender[1], Elke Pfaff[1], Sebastian Stark[1], Damien Faury[9], Jeremy Schwartzentruber[13], Jacek Majewski[13], Ursula D. Weber[10], Marc Zapatka[10], Benjamin Raeder[6], Matthias Schlesner[2], Catherine L. Worth[5], Cynthia C. Bartholomae[14], Christof von Kalle[14,15], Charles D. Imbusch[2], Sylwester Radomski[2,16,17], Chris Lawerenz[2], Peter van Sluis[18], Jan Koster[18], Richard Volckmann[18], Rogier Versteeg[18], Hans Lehrach[5], Camelia Monoranu[19], Beate Winkler[20], Andreas Unterberg[21], Christel Herold-Mende[21], Till Milde[12,22], Andreas E. Kulozik[12], Martin Ebinger[23], Martin U. Schuhmann[24], Yoon-Jae Cho[25], Scott L. Pomeroy[26,27], Andreas von Deimling[3,4], Olaf Witt[12,22], Michael D. Taylor[28], Stephan Wolf[11], Matthias A. Karajannis[29], Charles G. Eberhart[30], Wolfram Scheurlen[31], Martin Hasselblatt[32], Keith L.

Ligon[26,33,34], Mark W. Kieran[26,35], Jan O. Korbel[6], Marie-Laure Yaspo[5], Benedikt Brors[2], Jörg Felsberg[36], Guido Reifenberger[36], V. Peter Collins[7], Nada Jabado[9,37], Roland Eils[2,15,16,17,#], Peter Lichter[10,15,#], and Stefan M. Pfister[1,12,#] **On behalf of the ICGC PedBrain Tumor Project[38]**

Affiliations

[1]Division of Pediatric Neurooncology, German Cancer Research Center (DKFZ), Im Neuenheimer Feld 280, Heidelberg, 69120, Germany [2]Division of Theoretical Bioinformatics, German Cancer Research Center (DKFZ), Im Neuenheimer Feld 280, Heidelberg, 69120, Germany [3]Department of Neuropathology, University of Heidelberg, Im Neuenheimer Feld 224, Heidelberg, 69120, Germany [4]Clinical Cooperation Unit Neuropathology, German Cancer Research Center (DKFZ), Im Neuenheimer Feld 224, Heidelberg, 69120, Germany [5]Max Planck Institute for Molecular Genetics, Ihnestrasse 63–73, Berlin, 14195, Germany [6]European Molecular Biology Laboratory (EMBL), Genome Biology Unit, Meyerhofstrasse 1, Heidelberg, 69117, Germany [7]Division of Molecular Histopathology, Department of Pathology, University of Cambridge, Cambridge, CB2 0QQ, UK [8]Department of Neuropathology, Burdenko Neurosurgical Institute, 4th Tverskaya-Yamskaya 16, Moscow, 125047, Russia [9]Department of Human Genetics, McGill University, Montreal, Quebec, H3Z 2Z3, Canada [10]Division of Molecular Genetics, German Cancer Research Center (DKFZ), Im Neuenheimer Feld 280, Heidelberg, 69120, Germany [11]Genomics and Proteomics Core Facility, German Cancer Research Center (DKFZ), Im Neuenheimer Feld 280, Heidelberg, 69120, Germany [12]Department of Pediatric Oncology, Hematology & Immunology, Heidelberg University Hospital, Im Neuenheimer Feld 430, Heidelberg, 69120, Germany [13]McGill University and Genome Quebec Innovation Centre, Montreal, QC H3A 1A4, Canada [14]Division of Translational Oncology, German Cancer Research Center (DKFZ) and National Center for Tumor Diseases (NCT), Im Neuenheimer Feld 460, Heidelberg, 69120, Germany [15]Heidelberg Center for Personalised Oncology (DKFZ-HIPO), Heidelberg, 69120, Germany [16]Institute for Pharmacy and Molecular Biotechnology (IPMB), University of Heidelberg, Heidelberg, 69120, Germany [17]BioQuant Center, University of Heidelberg, Im Neuenheimer Feld 267, Heidelberg, 69120, Germany [18]Department of Oncogenomics, AMC, University of Amsterdam, Meibergdreef 9, Amsterdam, 1105 AZ, Netherlands [19]Department of Neuropathology, Institute of Pathology, Würzburg University, Josef-Schneider Strasse 2, Würzburg, 97080, Germany [20]Department of Pediatric Hematology and Oncology, Children's University Hospital Würzburg, Josef-Schneider-Straße 2, Würzburg, 97080, Germany [21]Department of Neurosurgery, Heidelberg University Hospital, Im Neuenheimer Feld 400, Heidelberg, 69120, Germany [22]Clinical Cooperation Unit Pediatric Oncology, German Cancer Research Center (DKFZ), Im Neuenheimer Feld 280, Heidelberg, 69120, Germany [23]Department of Hematology and Oncology, Children's University Hospital, Hoppe-Seyler Strasse 1, Tübingen, 72076, Germany [24]Department of Neurosurgery, University Hospital, Hoppe-Seyler Strasse 3, Tübingen, 72076, Germany [25]Division of Child Neurology, Stanford University, 750 Welch Road, Palo Alto, CA, 94304, USA [26]Boston Children's Hospital, 300 Longwood Avenue, Boston, MA, 02115, USA [27]Broad Institute of MIT and Harvard, Cambridge, MA, 02142, USA [28]Division of Neurosurgery and The Arthur and Sonia Labatt Brain Tumour Research Centre, Hospital for Sick Children, 555 University Avenue, Toronto, M5G 1X8, Canada [29]NYU Langone Medical Center, Hassenfeld Children's Center for Cancer and Blood Disorders, 160 East 32nd Street, New York, NY 10016, USA [30]Division of Pathology, Johns Hopkins University School of Medicine, 720 Rutland Ave, Ross Building 558, Baltimore, MD 21287, USA [31]Cnopf'sche Kinderklinik, Nürnberg Children's Hospital, St.-Johannis-

Mühlgasse 19, Nürnberg, 90419, Germany [32]Institute of Neuropathology, University Hospital Münster, Albert-Schweitzer-Campus 1, Münster, 48149, Germany [33]Center for Molecular Oncologic Pathology, Dana-Farber Cancer Institute, 450 Brookline Ave., Boston, MA 02215, USA [34]Department of Pathology, Brigham and Women's Hospital, 75 Francis Street, Boston, MA 02115, USA [35]Department of Pediatric Oncology, Dana-Farber Cancer Institute, 450 Brookline Ave., Boston, MA 02215, USA [36]Department of Neuropathology, Heinrich-Heine-University Düsseldorf, Moorenstrasse 5, Düsseldorf, 40225, Germany [37]Department of Paediatrics, Montreal Children's Hospital, McGill University Health Centre, Montreal, Quebec, H1P 2P3, Canada

Acknowledgments

For technical support and expertise we thank: Bettina Haase, Dinko Pavlinic, and Bianka Baying (EMBL genomics core facility); Michael Wahlers and Rupert Lück (EMBL high-performance computing facility); the DKFZ Genomics and Proteomics Core Facility; Malaika Knopf (NCT Heidelberg); Karin Schlangen, Macha Metsger, Kerstin Schulz, Asja Nürnberger, Alexander Kovacsovics, and Matthias Linser (Max Planck Institute for Molecular Genetics); Susanne Peetz-Dienhart and Yvonne Floer (University Hospital Münster); Danita M. Pearson (University of Cambridge) and Bingding Huang, Gideon Zipprich, Michael Heinold, Rolf Kabbe, Andrea Wittmann, Laura Sieber and Linda Linke (DKFZ). Walter Stummer (Münster), Bernd Hoffmann (Münster), Burkhard Rama, (Osnabrück), Heinrich Ebel (Hamm), Hans Axel Trost (Bayreuth) and Uwe Wildförster (Gelsenkirchen) provided detailed clinical information. We also thank GATC Biotech AG for sequencing services.

This work was principally supported by the PedBrain Tumor Project contributing to the International Cancer Genome Consortium, funded by German Cancer Aid (109252) and by the German Federal Ministry of Education and Research (BMBF, grants #01KU1201A, MedSys #0315416C and NGFN^{plus} #01GS0883). Additional support came from the German Cancer Research Center – Heidelberg Center for Personalized Oncology (DKFZ-HIPO), the Max Planck Society, Genome Canada and the Canadian Institute for Health Research (CIHR) with co-funding from Genome BC, Genome Quebec, CIHR-ICR (Institute for Cancer Research) and C17 (N. Jabado), Ian's Friend Foundation (M.A.K.), NIH grant numbers RO1CA105607 and P30HD018655 (S.L.P.), the Dutch Cancer Foundations KWF (2010-4713) and KIKA (M.Ko.), the Brain Tumour Charity (S.R.L. and V.P.C.) and the Pediatric Low Grade Astrocytoma Foundation (M.W.K. and K.L.L.).

References

1. Central Brain Tumor Registry of the United States. Statistical Report: Primary Brain and Central Nervous System Tumors Diagnosed in the United States, 2004–2008. CBTRUS; Hinsdale, IL: 2012.
2. Jones DTW, Gronych J, Lichter P, Witt O, Pfister SM. MAPK pathway activation in pilocytic astrocytoma. Cell Mol Life Sci. 2012; 69:1799–811. [PubMed: 22159586]
3. Gnekow AK, et al. Long-term follow-up of the multicenter, multidisciplinary treatment study HIT-LGG-1996 for low-grade glioma in children and adolescents of the German Speaking Society of Pediatric Oncology and Hematology. Neuro Oncol. 2012
4. Armstrong GT, et al. Survival and long-term health and cognitive outcomes after low-grade glioma. Neuro Oncol. 2011; 13:223–34. [PubMed: 21177781]
5. Schwartzentruber J, et al. Driver mutations in histone H3.3 and chromatin remodelling genes in paediatric glioblastoma. Nature. 2012; 482:226–31. [PubMed: 22286061]
6. Jones DTW, et al. Tandem duplication producing a novel oncogenic BRAF fusion gene defines the majority of pilocytic astrocytomas. Cancer Res. 2008; 68:8673–7. [PubMed: 18974108]
7. Jones DTW, et al. Oncogenic RAF1 rearrangement and a novel BRAF mutation as alternatives to KIAA1549:BRAF fusion in activating the MAPK pathway in pilocytic astrocytoma. Oncogene. 2009; 28:2119–23. [PubMed: 19363522]
8. Pfister S, et al. BRAF gene duplication constitutes a mechanism of MAPK pathway activation in low-grade astrocytomas. J Clin Invest. 2008
9. Gutmann DH, et al. Somatic neurofibromatosis type 1 (NF1) inactivation characterizes NF1-associated pilocytic astrocytoma. Genome Res. 2013; 23:431–9. [PubMed: 23222849]

10. Jones DTW, et al. Dissecting the genomic complexity underlying medulloblastoma. Nature. 2012; 488:100–5. [PubMed: 22832583]
11. Pugh TJ, et al. Medulloblastoma exome sequencing uncovers subtype-specific somatic mutations. Nature. 2012; 488:106–10. [PubMed: 22820256]
12. Robinson G, et al. Novel mutations target distinct subgroups of medulloblastoma. Nature. 2012; 488:43–8. [PubMed: 22722829]
13. Downing JR, et al. The Pediatric Cancer Genome Project. Nat Genet. 2012; 44:619–22. [PubMed: 22641210]
14. Stephens PJ, et al. The landscape of cancer genes and mutational processes in breast cancer. Nature. 2012; 486:400–4. [PubMed: 22722201]
15. Welch JS, et al. The origin and evolution of mutations in acute myeloid leukemia. Cell. 2012; 150:264–78. [PubMed: 22817890]
16. Cin H, et al. Oncogenic FAM131B-BRAF fusion resulting from 7q34 deletion comprises an alternative mechanism of MAPK pathway activation in pilocytic astrocytoma. Acta Neuropathol. 2011; 121:763–74. [PubMed: 21424530]
17. Wan PT, et al. Mechanism of activation of the RAF-ERK signaling pathway by oncogenic mutations of B-RAF. Cell. 2004; 116:855–67. [PubMed: 15035987]
18. Rushworth LK, Hindley AD, O'Neill E, Kolch W. Regulation and role of Raf-1/B-Raf heterodimerization. Mol Cell Biol. 2006; 26:2262–72. [PubMed: 16508002]
19. Terai K, Matsuda M. The amino-terminal B-Raf-specific region mediates calcium-dependent homo- and hetero-dimerization of Raf. EMBO J. 2006; 25:3556–64. [PubMed: 16858395]
20. Macedo MP, et al. Multiple mutations in the Kras gene in colorectal cancer: review of the literature with two case reports. Int J Colorectal Dis. 2011; 26:1241–8. [PubMed: 21603900]
21. Naguib A, Wilson CH, Adams DJ, Arends MJ. Activation of K-RAS by co-mutation of codons 19 and 20 is transforming. J Mol Signal. 2011; 6:2. [PubMed: 21371307]
22. Schramm A, et al. Biological effects of TrkA and TrkB receptor signaling in neuroblastoma. Cancer Lett. 2005; 228:143–53. [PubMed: 15921851]
23. Thiele CJ, Li Z, McKee AE. On Trk--the TrkB signal transduction pathway is an increasingly important target in cancer biology. Clin Cancer Res. 2009; 15:5962–7. [PubMed: 19755385]
24. Greco A, Miranda C, Pierotti MA. Rearrangements of NTRK1 gene in papillary thyroid carcinoma. Mol Cell Endocrinol. 2010; 321:44–9. [PubMed: 19883730]
25. Lannon CL, Sorensen PH. ETV6-NTRK3: a chimeric protein tyrosine kinase with transformation activity in multiple cell lineages. Semin Cancer Biol. 2005; 15:215–23. [PubMed: 15826836]
26. Dewitt J, et al. Constitutively active TrkB confers an aggressive transformed phenotype to a neural crest-derived cell line. Oncogene. 2013
27. Kaplan DR, Miller FD. Neurotrophin signal transduction in the nervous system. Curr Opin Neurobiol. 2000; 10:381–91. [PubMed: 10851172]
28. Theillet C, et al. FGFRI and PLAT genes and DNA amplification at 8p12 in breast and ovarian cancers. Genes Chromosomes Cancer. 1993; 7:219–26. [PubMed: 7692948]
29. Dutt A, et al. Inhibitor-sensitive FGFR1 amplification in human non-small cell lung cancer. PLoS One. 2011; 6:e20351. [PubMed: 21666749]
30. Weiss J, et al. Frequent and focal FGFR1 amplification associates with therapeutically tractable FGFR1 dependency in squamous cell lung cancer. Sci Transl Med. 2010; 2:62ra93.
31. Rand V, et al. Sequence survey of receptor tyrosine kinases reveals mutations in glioblastomas. Proc Natl Acad Sci U S A. 2005; 102:14344–9. [PubMed: 16186508]
32. TCGA. Comprehensive genomic characterization defines human glioblastoma genes and core pathways. Nature. 2008; 455:1061–8. [PubMed: 18772890]
33. Singh D, et al. Transforming fusions of FGFR and TACC genes in human glioblastoma. Science. 2012; 337:1231–5. [PubMed: 22837387]
34. Forbes SA, et al. COSMIC: mining complete cancer genomes in the Catalogue of Somatic Mutations in Cancer. Nucleic Acids Res. 2011; 39:D945–50. [PubMed: 20952405]
35. Liu A, et al. FGF17b and FGF18 have different midbrain regulatory properties from FGF8b or activated FGF receptors. Development. 2003; 130:6175–85. [PubMed: 14602678]

36. Lew ED, Furdui CM, Anderson KS, Schlessinger J. The precise sequence of FGF receptor autophosphorylation is kinetically driven and is disrupted by oncogenic mutations. Sci Signal. 2009; 2:ra6. [PubMed: 19224897]
37. Yoon K, et al. Fibroblast growth factor receptor signaling promotes radial glial identity and interacts with Notch1 signaling in telencephalic progenitors. J Neurosci. 2004; 24:9497–506. [PubMed: 15509736]
38. Gravendeel LA, et al. Intrinsic gene expression profiles of gliomas are a better predictor of survival than histology. Cancer Res. 2009; 69:9065–72. [PubMed: 19920198]
39. Sturm D, et al. Hotspot Mutations in H3F3A and IDH1 Define Distinct Epigenetic and Biological Subgroups of Glioblastoma. Cancer Cell. 2012; 22:425–37. [PubMed: 23079654]
40. Roth RB, et al. Gene expression analyses reveal molecular relationships among 20 regions of the human CNS. Neurogenetics. 2006; 7:67–80. [PubMed: 16572319]
41. Breitenbuecher F, et al. Identification of a novel type of ITD mutations located in nonjuxtamembrane domains of the FLT3 tyrosine kinase receptor. Blood. 2009; 113:4074–7. [PubMed: 18483393]
42. Tartaglia M, et al. Somatic mutations in PTPN11 in juvenile myelomonocytic leukemia, myelodysplastic syndromes and acute myeloid leukemia. Nat Genet. 2003; 34:148–50. [PubMed: 12717436]
43. Chan G, Kalaitzidis D, Neel B. The tyrosine phosphatase Shp2 (*PTPN11*) in cancer. Cancer and Metastasis Reviews. 2008; 27:179–192. [PubMed: 18286234]
44. Romano AA, et al. Noonan syndrome: clinical features, diagnosis, and management guidelines. Pediatrics. 2010; 126:746–59. [PubMed: 20876176]
45. Tartaglia M, Gelb BD. Noonan syndrome and related disorders: genetics and pathogenesis. Annu Rev Genomics Hum Genet. 2005; 6:45–68. [PubMed: 16124853]
46. Fryssira H, et al. Tumor development in three patients with Noonan syndrome. Eur J Pediatr. 2008; 167:1025–31. [PubMed: 18057963]
47. Sanford RA, Bowman R, Tomita T, De Leon G, Palka P. A 16-year-old male with Noonan's syndrome develops progressive scoliosis and deteriorating gait. Pediatr Neurosurg. 1999; 30:47–52. [PubMed: 10202309]
48. Schuettpelz LG, et al. Pilocytic astrocytoma in a child with Noonan syndrome. Pediatr Blood Cancer. 2009; 53:1147–9. [PubMed: 19621452]
49. Vulpoi C, et al. LEOPARD syndrome and pilocytic astrocytome: a random association? Endocrine Abstracts. 2009; 20
50. Zenker M. Clinical manifestations of mutations in RAS and related intracellular signal transduction factors. Curr Opin Pediatr. 2011; 23:443–51. [PubMed: 21750428]
51. Gronych J, et al. An activated mutant BRAF kinase domain is sufficient to induce pilocytic astrocytoma in mice. J Clin Invest. 2011; 121:1344–8. [PubMed: 21403401]
52. Kaul A, Chen YH, Emnett RJ, Dahiya S, Gutmann DH. Pediatric glioma-associated KIAA1549:BRAF expression regulates neuroglial cell growth in a cell type-specific and mTOR-dependent manner. Genes Dev. 2012; 26:2561–6. [PubMed: 23152448]
53. Khuong-Quang DA, et al. K27M mutation in histone H3.3 defines clinically and biologically distinct subgroups of pediatric diffuse intrinsic pontine gliomas. Acta Neuropathol. 2012; 124:439–47. [PubMed: 22661320]
54. Agazie YM, Hayman MJ. Molecular mechanism for a role of SHP2 in epidermal growth factor receptor signaling. Mol Cell Biol. 2003; 23:7875–86. [PubMed: 14560030]
55. Ma DK, Ponnusamy K, Song MR, Ming GL, Song H. Molecular genetic analysis of FGFR1 signalling reveals distinct roles of MAPK and PLCgamma1 activation for self-renewal of adult neural stem cells. Mol Brain. 2009; 2:16. [PubMed: 19505325]
56. Tole S, Gutin G, Bhatnagar L, Remedios R, Hebert JM. Development of midline cell types and commissural axon tracts requires Fgfr1 in the cerebrum. Dev Biol. 2006; 289:141–51. [PubMed: 16309667]
57. Lee DY, Gianino SM, Gutmann DH. Innate neural stem cell heterogeneity determines the patterning of glioma formation in children. Cancer Cell. 2012; 22:131–8. [PubMed: 22789544]

58. Lee DY, Yeh TH, Emnett RJ, White CR, Gutmann DH. Neurofibromatosis-1 regulates neuroglial progenitor proliferation and glial differentiation in a brain region-specific manner. Genes Dev. 2010; 24:2317–29. [PubMed: 20876733]
59. Jacob K, et al. Genetic aberrations leading to MAPK pathway activation mediate oncogene-induced senescence in sporadic pilocytic astrocytomas. Clin Cancer Res. 2011
60. Raabe EH, et al. BRAF Activation Induces Transformation and Then Senescence in Human Neural Stem Cells: A Pilocytic Astrocytoma Model. Clin Cancer Res. 2011; 17:3590–9. [PubMed: 21636552]
61. Sievert AJ, et al. Paradoxical activation and RAF inhibitor resistance of BRAF protein kinase fusions characterizing pediatric astrocytomas. Proc Natl Acad Sci U S A. 2013; 110:5957–62. [PubMed: 23533272]
62. Dieci MV, Arnedos M, Andre F, Soria JC. Fibroblast growth factor receptor inhibitors as a cancer treatment: from a biologic rationale to medical perspectives. Cancer Discov. 2013; 3:264–79. [PubMed: 23418312]
63. Iyer R, et al. AZ64 inhibits TrkB and enhances the efficacy of chemotherapy and local radiation in neuroblastoma xenografts. Cancer Chemother Pharmacol. 2012; 70:477–86. [PubMed: 22623209]
64. Rusconi P, Caiola E, Broggini M. RAS/RAF/MEK inhibitors in oncology. Curr Med Chem. 2012; 19:1164–76. [PubMed: 22257058]
65. Parkhomchuk D, et al. Transcriptome analysis by strand-specific sequencing of complementary DNA. Nucleic Acids Res. 2009; 37(18):e123. [PubMed: 19620212]
66. Sultan M, et al. A simple strand-specific RNA-Seq library preparation protocol combining the Illumina TruSeq RNA and the dUTP methods. Biochem Biophys Res Commun. 2012; 422(4): 643–6. [PubMed: 22609201]
67. Li H, Durbin R. Fast and accurate short read alignment with Burrows-Wheeler transform. Bioinformatics. 2009; 25 (14):1754–60. [PubMed: 19451168]
68. Li H, et al. The Sequence Alignment/Map format and SAMtools. Bioinformatics. 2009; 25 (16): 2078–2079. [PubMed: 19505943]
69. Ye K, Schulz MH, Long Q, Apweiler R, Ning Z. Pindel: a pattern growth approach to detect break points of large deletions and medium sized insertions from paired-end short reads. Bioinformatics. 2009; 25:2865–2871. [PubMed: 19561018]
70. Wang K, et al. ANNOVAR: functional annotation of genetic variants from high-throughput sequencing data. Nucleic Acids Res. 2010; 38 (16):e164. [PubMed: 20601685]
71. Dees ND, et al. MuSiC: identifying mutational significance in cancer genomes. Genome Res. 2012; 22:1589–98. [PubMed: 22759861]
72. Nik-Zainal S, et al. Mutational Processes Molding the Genomes of 21 Breast Cancers. Cell. 2012; 149:979–993. [PubMed: 22608084]
73. Quinlan AR, Hall IM. BEDTools: a flexible suite of utilities for comparing genomic features. Bioinformatics. 2010; 26:841–842. [PubMed: 20110278]
74. Wang J, et al. CREST maps somatic structural variation in cancer genomes with base-pair resolution. Nat Methods. 2011; 8(8):652–4. [PubMed: 21666668]
75. Rausch T, et al. DELLY: structural variant discovery by integrated paired-end and split-read analysis. Bioinformatics. 2012; 28 (18):i333–i339. [PubMed: 22962449]
76. Kim D, Salzberg SL. TopHat-Fusion: an algorithm for discovery of novel fusion transcripts. Genome Biol. 2011; 12(8):R72. [PubMed: 21835007]
77. McPherson A, et al. deFuse: an algorithm for gene fusion discovery in tumor RNA-Seq data. PLoS Comput Biol. 2011; 7(5):e1001138. [PubMed: 21625565]
78. Sali A, Blundell TL. Comparative protein modelling by satisfaction of spatial restraints. J Mol Biol. 1993; 234:779–815. [PubMed: 8254673]

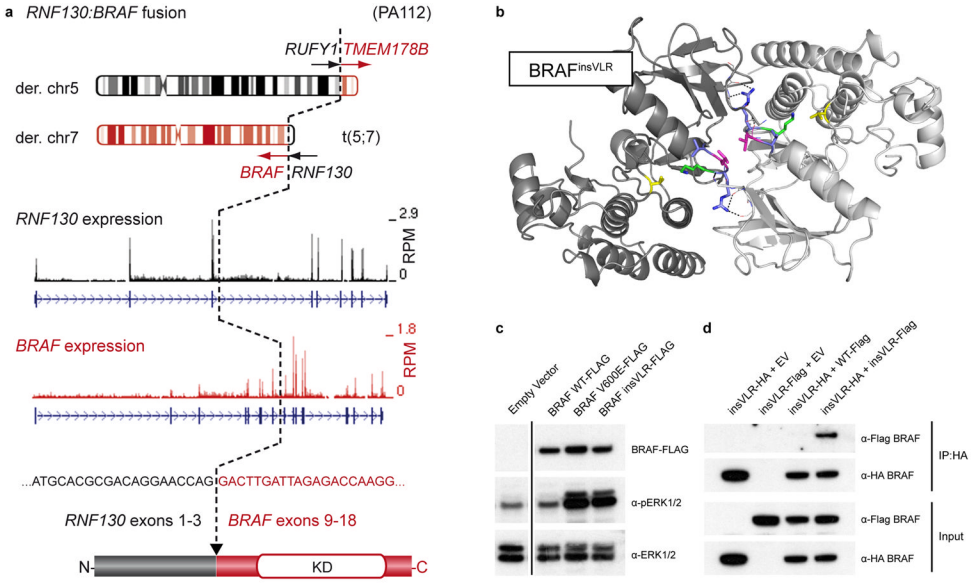

Figure 1. Novel *BRAF* alterations in pilocytic astrocytoma

a, Schematic representation of the *RNF130:BRAF* fusion gene in ICGC_PA112 resulting from a translocation between chromosomes 5 and 7. A similar fusion was observed in ICGC_PA96. The cDNA sequence at the fusion breakpoint and resulting exon and protein structures are indicated. A reciprocal fusion between *RUN and FYVE domain containing 1* (*RUFY1*) and *transmembrane protein 178B* (*TMEM178B*) on the derivative chromosome 5 in ICGC_PA112 was also found to be expressed by RNA-seq analysis (not shown). RPM, reads per million; KD, kinase domain.

b, Computational modeling of two BRAF monomers (light/dark grey) with a VLR insertion (blue/magenta) between Arg506 and Lys507 (green), as identified in ICGC_PA65. The PDB structure 4E26 was used as a template. Val600, a mutational hotspot, is shown in yellow. A novel dimer interface is formed between the protomers, with hydrogen bonds from the new arginine side chains (dashed lines) and a hydrophobic interaction between the leucine side chains (magenta).

c, Western blot analysis of NIH3T3 cells transfected with empty vector (EV), $BRAF^{WT}$, $BRAF^{V600E}$ and $BRAF^{insVLR}$. The newly identified insVLR mutant results in elevation of ERK1/2 phosphorylation (pERK1/2) at a similar level to that seen with the known oncogenic V600E form.

d, Co-immunoprecipation assay with pull-down of HA-tagged $BRAF^{insVLR}$, demonstrating that this novel mutant forms homodimers with co-transfected AU1-tagged insVLR, but does not appear to form a strong heterodimer with wild-type BRAF.

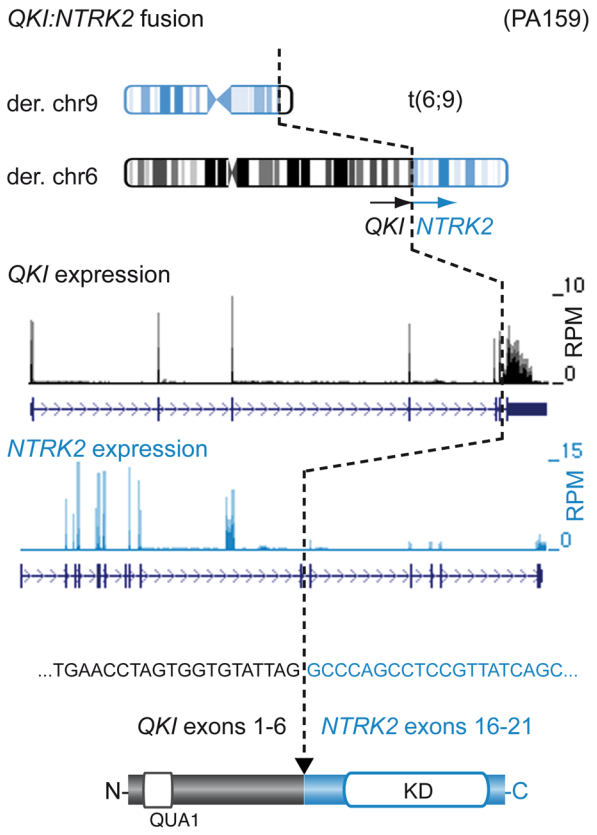

Figure 2. *NTRK2* is a new gene fusion target in pilocytic astrocytoma

Schematic representation of the *QKI:NTRK2* fusion gene in ICGC_PA159 resulting from a translocation between chromosomes 6 and 9. A similar fusion was observed in ICGC_PA82. The cDNA sequence at the fusion breakpoint and resulting exon and protein structures are indicated. RPM, reads per million; KD, kinase domain; QUA1, Qua1 dimerization domain.

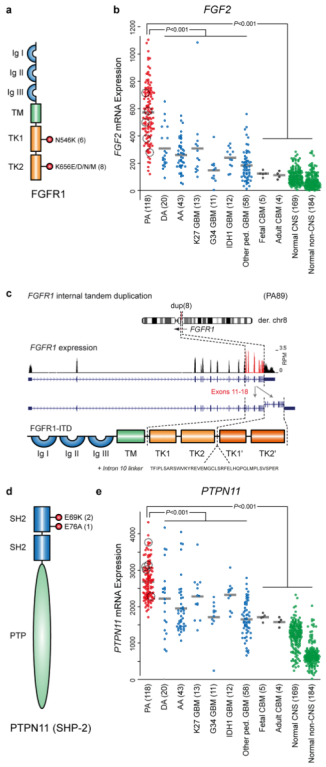

Figure 3. FGF pathway signaling molecules are recurrently altered in pilocytic astrocytoma

a, Schematic of the domain structure of FGFR1, indicating the position and frequency of the hotspot mutations in pilocytic astrocytomas sequenced in the present study (including replication cases).

b, Gene expression data for *FGF2* indicating significantly elevated expression in pilocytic astrocytomas (red) compared with other astrocytic tumors (blue), normal cerebellum (black) or other normal tissues (green); $P < 0.001$, two-sided t-test. The pilocytic astrocytomas with expression data which harbor *FGFR1* alterations (four mutants plus FGFR1-ITD) are highlighted.

c, Schematic of an additional alteration in *FGFR1* identified in ICGC_PA89, comprising an internal tandem duplication (ITD) of part of intron 10, exons 11–17 and part of exon 18. The duplicated amino acids are aa478–820 (numbered according to the alpha A1 isoform), with an additional 40 amino acid linker sequence encoded by part of intron 10. The whole kinase domain is therefore duplicated in the resulting predicted protein (TK1′ and TK2′).

d, Schematic of the structure of PTPN11 (SHP-2), indicating the position and frequency of mutations in pilocytic astrocytomas sequenced in the present study.

e, Gene expression data for *PTPN11* indicating significantly elevated expression in pilocytic astrocytomas compared with other groups, as in (b); $P < 0.001$, two-sided t-test. The pilocytic astrocytomas with expression data which harbor *FGFR1* alterations (four mutants plus FGFR1-ITD) are highlighted.

Ig, immunoglobulin-like domain; TM, transmembrane domain; TK, tyrosine kinase domain; SH2, src homology 2 domain; PTP, protein tyrosine phosphatase domain; DA, WHO Grade II diffuse astrocytoma; AA, anaplastic astrocytoma; K27/G34/IDH1 GBM, glioblastoma carrying a mutation at K27 or G34 in H3F3A or in IDH1; ped., pediatric; CBM, cerebellum, CNS, central nervous system.

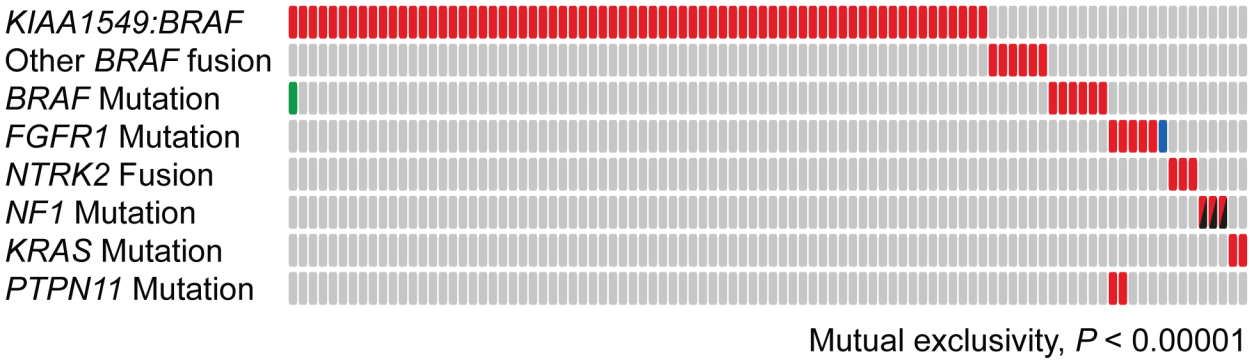

Figure 4. Summary of MAPK pathway alterations in pilocytic astrocytoma

An overview of MAPK pathway alterations identified in the 96 whole-genome sequencing cases included in the present study, indicating the mutual exclusivity of the majority of these hits (with the exception of *FGFR1* and *PTPN11*); P <0.0001, permutation test on 10,000 iterations. Each column represents one tumor sample. Red filled boxes indicate that a given alteration is present in this sample. The blue filled box represents FGFR1-ITD rather than a point mutation; the green box indicates a $BRAF^{E451D}$ mutation in a case with a *KIAA1549:BRAF* fusion (unknown functional significance, but included in the exclusivity testing); the black/red boxes indicate that the *NF1* alterations comprise one germline and one somatic hit per case.